A Hybrid Atmospheric Model Incorporating Machine Learning Can Capture Dynamical Processes Not Captured by Its Physics-Based Component

Troy Arcomano[1*], Istvan Szunyogh[1], Alexander Wikner[2], Brian R. Hunt[3], and Edward Ott[2,4]

[1]Department of Atmospheric Sciences, Texas A&M University, College Station, TX, USA
[2]Department of Physics, University of Maryland, College Park, MD, USA
[3]Institute for Physical Science and Technology, University of Maryland, College Park, MD, USA
[4]Department of Electrical and Computer Engineering, University of Maryland, College Park, MD, USA

Key Points:

- A hybrid system combining an AGCM with a machine-learning component can capture processes not captured by the AGCM.
- Machine learning provides a flexible framework to introduce additional prognostic variables into the hybrid model.
- The prototype hybrid model tested in the paper is stable and has a realistic climate in decades-long simulation experiments.

[*]Current address, Argonne National Laboratory

Corresponding author: Troy Arcomano, tarcomano@anl.gov

Abstract

It is shown that a recently developed hybrid modeling approach that combines machine learning (ML) with an atmospheric global circulation model (AGCM) can serve as a basis for capturing atmospheric processes not captured by the AGCM. This power of the approach is illustrated by three examples from a decades-long climate simulation experiment. The first example demonstrates that the hybrid model can produce sudden stratospheric warming (SSW), a dynamical process of nature not resolved by the low resolution AGCM component of the hybrid model. The second and third example show that introducing 6-h cumulative precipitation and sea surface temperature (SST) as ML-based prognostic variables improves the precipitation climatology and leads to a realistic ENSO signal in the SST and atmospheric surface pressure.

Plain Language Summary

This paper introduces and tests schemes for efficiently enabling significant expansion of the utility and scope of a recently introduced hybrid modeling technique that combines machine learning with an atmospheric global circulation model (AGCM). Simulation experiments are carried out with an implementation of the approach on a low resolution simplified AGCM. An examination of the simulated atmospheric circulation suggests that the hybrid model can capture dynamical process not captured by the AGCM. Moreover, the addition of precipitation and sea surface temperature as machine learning predicted physical quantities to the model improves the precipitation climatology and leads to a realistic El Niño-La Niña signal in the SST and atmospheric surface pressure.

1 Introduction

Arcomano et al. (2022) (AEA22 hereafter) described a hybrid atmospheric modeling approach that combines machine learning (ML) with an atmospheric general circulation model (AGCM). They showed that, when the hybrid model was used for weather prediction, it provided more accurate short and medium range (1-7 days) forecasts than either the AGCM or the ML-only component of the model (Arcomano et al., 2020) acting alone. They also showed that when the model was used for climate simulations, it greatly reduced the systematic errors (biases) of the model climate compared to that of the AGCM. In the present study, we further explore the potential of the approach of AEA22 for climate modeling, and describe methods that significantly extends its utility and scope. The results we report are in accord with the idea that the inaccuracies of an AGCM could potentially be mitigated by utilization of information in time series of past observational data via the ML component of the hybrid.

The approach of AEA22 is an implementation of the combined hybrid/parallel prediction (CHyPP) scheme of Wikner et al. (2020) on an AGCM. CHyPP itself is an adaptation of the hybrid modeling approach of Pathak, Wikner, et al. (2018) to large dynamical systems, using the parallel reservoir computing (RC) algorithm of Pathak, Hunt, et al. (2018) for ML. Other hybrid approaches recently proposed for earth system modeling (Brenowitz & Bretherton, 2018, 2019; Rasp et al., 2018; Chattopadhyay et al., 2020; Farchi et al., 2021; Gentine et al., 2018; Watt-Meyer et al., 2021; Clark et al., 2022) use either random forests or deep learning for ML.

Section 2 summarizes the approach of AEA22 and explains how additional prognostic variables can be introduced into the hybrid model without changing the AGCM. Section 3 demonstrates the potential of the approach by three examples from a climate simulation experiment. The first example, the presence of sudden stratospheric warming (SSW) events, illustrates that the hybrid model can capture some dynamical processes of nature not resolved by the AGCM. The second and third example, realistic precipitation climatology and SST variability, demonstrate that some other dynamical pro-

cesses can be reproduced by modifying the AEA22 hybrid via addition of new ML-based prognostic variables (precipitation and sea surface temperature). As in AEA22, the AGCM of the simulation experiments is the Simplified Parameterization, primitive-Equation Dynamics (SPEEDY) model (Kucharski et al., 2006; Molteni, 2003).

2 The Hybrid Modeling Approach

2.1 The Hybrid Modeling Approach of AEA22

The hybrid model uses the same computational grid as the AGCM. The elements of the hybrid global state vector $\mathbf{v}_G^H(t)$ and physics-based global state vector $\mathbf{v}_G^P(t)$ are the grid-point values of the prognostic model variables. The input of the "one-time-step" hybrid global model solution $\mathbf{v}_G^H(t+\Delta t)$ is $\mathbf{v}_G^H(t)$, where the "time step" Δt is significantly longer than the time step of the AGCM. No changes are made to the AGCM, which is started from $\mathbf{v}_G^H(t)$ to provide the physics-based contribution $\mathbf{v}_G^P(t+\Delta t)$ to $\mathbf{v}_G^H(t+\Delta t)$. The hybridization is done by subdividing the global atmosphere into L local regions and obtaining a hybrid local model solution for each region. The computations for the different local regions ($\ell = 1, 2, \ldots, L$) are carried out in parallel and $\mathbf{v}_G^H(t+\Delta t)$ is obtained by assembling the hybrid local solutions. The next paragraph outlines the calculations that provide the hybrid local model solution for local region ℓ.

The elements of the physics based local state vector $\check{\mathbf{v}}_\ell^P(t+\Delta t)$ are the standardized elements of $\mathbf{v}_G^P(t+\Delta t)$ that fall into local region ℓ. (Hereafter, the symbol $\check{\mathbf{x}}$ indicates a standardized vector obtained by subtracting a related mean value and dividing by a related standard deviation for each element of $\mathbf{x}$.) The "one-time-step" hybrid local model solution is

$$\check{\mathbf{v}}_\ell^H(t+\Delta t) = \mathbf{W}_\ell \begin{pmatrix} \check{\mathbf{v}}_\ell^P(t+\Delta t) \\ \tilde{\mathbf{r}}_\ell(t+\Delta t) \end{pmatrix}, \tag{1}$$

where $\mathbf{W}_\ell$ is a weight matrix whose entries are to be determined by ML training, which will be discussed in Sec. 2.2. The D_r-dimensional vector $\tilde{\mathbf{r}}_\ell(t+\Delta t)$ is a quadratic function of the reservoir state vector $\mathbf{r}_\ell(t+\Delta t)$, where the reservoir is a dynamical system with evolution equation (Jaeger, 2001; Lukoševičius & Jaeger, 2009; Lukoševičius, 2012)

$$\mathbf{r}_\ell(t+\Delta t) = \tanh\left[\mathbf{A}_\ell \mathbf{r}_\ell(t) + \mathbf{B}_\ell \check{\mathbf{u}}_\ell(t)\right]. \tag{2}$$

Each entry of the $D_r \times D_r$ weighted adjacency matrix $\mathbf{A}_\ell$ is randomly chosen with a probability κ/D_r of being nonzero and assigned a random value chosen uniformly in $(0, 1]$. The nonzero entries are scaled such that the magnitude of the largest eigenvalue of $\mathbf{A}_\ell$ has a prescribed value ρ ($0 < \rho < 1$), called the spectral radius. The D_u-dimensional vector $\check{\mathbf{u}}_\ell(t)$ is the input vector of the reservoir, whose elements are standardized elements of the global hybrid state vector $\mathbf{v}_G^H(t)$ from an extended local region that has overlaps with its four neighbors. $\mathbf{B}_\ell$ is a matrix with entries chosen randomly on the interval $(-\alpha, \alpha)$, where α is an adjustable parameter. The hybrid local model solution is obtained by transforming the standardized values of the elements of $\check{\mathbf{v}}_\ell^H(t+\Delta t)$ to non-standardized values.

The initial value of $\mathbf{v}_G^H(0)$ at the beginning of a forecast or simulation is a conventional observational analysis $\mathbf{v}_G^A(0)$ for the AGCM. Starting the hybrid model also requires an initial value $\mathbf{r}_\ell(0)$ for each of the L reservoir state vectors. These initial values are obtained using Equation 2 to synchronize the evolution of the reservoirs with the atmospheric states for a short period prior ($t < 0$) to the start time of the forecast or simulation. This synchronization is achieved by feeding the reservoirs input vectors based on observational analyses for the synchronization period.

2.2 Training the Hybrid Model

The machine-learning component of the model learns to predict $\breve{\mathbf{v}}_\ell^H(t+\Delta t)$ from $\mathbf{v}_G^H(t)$ for each local region by training. The training data are based on global observational analyses $\mathbf{v}_G^A(t)$. These analyses provide the initial conditions for the Δt-long AGCM forecasts and are standardized and restricted to the extended local region to form the input $\mathbf{u}_\ell(t)$ for each of the L reservoirs. To promote stability, a small-magnitude random noise $\varepsilon(k\Delta t)$ is introduced into the analyses before forming the input vectors by the formula $[1+\varepsilon(k\Delta t)]\mathbf{v}_G^A(k\Delta t)$.

The training data after standardization also provide the elements of the desired outcome $\breve{\mathbf{v}}_\ell^A(t+\Delta t)$ to which $\breve{\mathbf{v}}_\ell^H(t+\Delta t)$ can be compared during training. Formally, the training seeks the weight matrix $\mathbf{W}_\ell$ for which the "one-time-step" predictions $\breve{\mathbf{v}}_\ell^H(k\Delta t, \mathbf{W}_\ell)$ $(k=-K+1,-K+2,\ldots,0)$ best fit $\breve{\mathbf{v}}_\ell^A(k\Delta t)$ in a least-square sense. That is, $\mathbf{W}_\ell$ is the minimizer of the quadratic cost-function

$$J(\mathbf{W}_\ell)=\sum_{k=-K+1}^{0}\|\breve{\mathbf{v}}_\ell^H(k\Delta t,\mathbf{W}_\ell)-\breve{\mathbf{v}}_\ell^A(k\Delta t)\|^2+\beta^P\|\mathbf{W}^P\|^2+\beta^R\|\mathbf{W}^R\|^2, \tag{3}$$

where $\mathbf{W}^P$ and $\mathbf{W}^R$ are matrices for which

$$\breve{\mathbf{v}}_\ell^H(t+\Delta t)=\mathbf{W}_\ell^P\breve{\mathbf{v}}_\ell^P(t+\Delta t)+\mathbf{W}_\ell^R\tilde{\mathbf{r}}_\ell(t+\Delta t),\qquad \mathbf{W}_\ell=\begin{pmatrix}\mathbf{W}_\ell^P & \mathbf{W}_\ell^R\end{pmatrix}, \tag{4}$$

is equivalent to Equation 1. The adjustable parameters β^P and β^R are chosen regularization parameters (Tikhonov and Arsenin 1977). It can be shown that the direct solution of the minimization problem is the matrix

$$\mathbf{W}_\ell=\begin{pmatrix}\mathbf{V}_\ell^A\left(\mathbf{V}_\ell^P\right)^T & \mathbf{V}_\ell^A\tilde{\mathbf{R}}_\ell^T\end{pmatrix}\begin{pmatrix}\mathbf{V}_\ell^P\left(\mathbf{V}_\ell^P\right)^T+\beta^P\mathbf{I} & \mathbf{V}_\ell^P\tilde{\mathbf{R}}_\ell^T\\ \tilde{\mathbf{R}}_\ell\left(\mathbf{V}_\ell^P\right)^T & \tilde{\mathbf{R}}_\ell\tilde{\mathbf{R}}_\ell^T+\beta^R\mathbf{I}\end{pmatrix}^{-1}. \tag{5}$$

In this equation, column k of the matrix $\mathbf{V}_\ell^P$ is the local state vector $\breve{\mathbf{v}}_\ell^P(k\Delta t)$ that corresponds to the physics-based model solution $\mathbf{v}_G^P(k\Delta t)$ started from $\mathbf{v}_G^A[(k-1)\Delta t]$, column k of the matrix $\tilde{\mathbf{R}}_\ell$ is $\tilde{\mathbf{r}}_\ell(k\Delta t)$, and column k of the matrix $\mathbf{V}_\ell^A$ is $\breve{\mathbf{v}}_\ell^A(k\Delta t)$.

2.3 Introducing New ML-Based Prognostic Variables

In atmospheric modeling, the term 'prognostic variable' refers to a state variable whose temporal evolution is predicted directly by a model equation. The hybrid approach provides a framework for introducing new prognostic variables without making any changes to the AGCM provided that training data are available for the new variables. Two specific methods that take advantage of this flexibility are described here: Method I is designed for atmospheric variables that are not required to evolve the ACGM; while Method II is designed for external variables, variables represented by prescribed boundary fields in a standalone ACGM, which might vary on a different time scale than the atmospheric prognostic variables.

2.3.1 Method I

The purpose of Method I is to introduce a prognostic variable that is either not predicted by the AGCM, or predicted only indirectly as a 'byproduct' of the parameterization schemes. This approach will be demonstrated by introducing precipitation as a prognostic variable (Section 3).

Let

$$\mathbf{v}_G^{H+}(t+\Delta t)=\begin{pmatrix}\mathbf{v}_G^H(t+\Delta t)\\ \mathbf{v}_G^{H*}(t+\Delta t)\end{pmatrix} \tag{6}$$

be the global state vector of hybrid model, where $\mathbf{v}_G^{H*}(t)$ represents the global field of a new prognostic variable. The corresponding local state vector for local region ℓ is

$$\breve{\mathbf{v}}_\ell^{H+}(t+\Delta t) = \begin{pmatrix} \breve{\mathbf{v}}_\ell^{H}(t+\Delta t) \\ \breve{\mathbf{v}}_\ell^{H*}(t+\Delta t) \end{pmatrix}. \tag{7}$$

The equation of the reservoir dynamics is modified as

$$\mathbf{r}_\ell^{+}(t+\Delta t) = \tanh\left[\mathbf{A}_\ell \mathbf{r}_\ell^{+}(t) + \mathbf{B}_\ell \breve{\mathbf{u}}_\ell^{+}(t)\right], \tag{8}$$

where $\breve{\mathbf{u}}_\ell^{+}(t)$ is an extended local state vector, which also includes the grid-point values of the new prognostic variable from the extended local region. In addition, Equation 4 is modified as

$$\breve{\mathbf{v}}_\ell^{H+}(t+\Delta t) = \begin{pmatrix} \breve{\mathbf{v}}_\ell^{H}(t+\Delta t) \\ \breve{\mathbf{v}}_\ell^{H*}(t+\Delta t) \end{pmatrix} = \begin{pmatrix} \mathbf{W}_\ell^{P} \\ \mathbf{W}_\ell^{P*} \end{pmatrix} \breve{\mathbf{v}}_\ell^{P}(t+\Delta t) + \begin{pmatrix} \mathbf{W}_\ell^{R} \\ \mathbf{W}_\ell^{R*} \end{pmatrix} \tilde{\mathbf{r}}_\ell^{+}(t+\Delta t)$$

which leads to the following modification of Equation 1:

$$\begin{aligned} \breve{\mathbf{v}}_\ell^{H+}(t+\Delta t) &= \begin{pmatrix} \breve{\mathbf{v}}_\ell^{H+}(t+\Delta t) \\ \breve{\mathbf{v}}_\ell^{H*}(t+\Delta t) \end{pmatrix} = \mathbf{W}_\ell \begin{pmatrix} \breve{\mathbf{v}}_\ell^{P}(t+\Delta t) \\ \tilde{\mathbf{r}}_\ell^{+}(t+\Delta t) \end{pmatrix} \\ \mathbf{W}_\ell &= \begin{pmatrix} \mathbf{W}_\ell^{P} & \mathbf{W}_\ell^{R} \\ \mathbf{W}_\ell^{P*} & \mathbf{W}_\ell^{R*} \end{pmatrix}. \end{aligned} \tag{9}$$

2.3.2 Method II

In an AGCM, the effects of the other earth system components, such as the ocean, cryosphere, land, and biosphere on the atmosphere are taken into account by parameterization schemes that include fields of some state variables of the other components at the earth's surface as input. In a standalone AGCM these fields must be prescribed. For instance, the thermal effects of the ocean on the atmosphere are taken into account by schemes that include prescribed SST fields, which are based on past SST observational analyses in the case of a climate simulation, or the latest SST analysis in the case of a weather forecast. A limitation of this approach is that it does not take into account feedbacks from the state variables of the AGCM to the prescribed state variables. Method II addresses this issue by replacing a prescribed field with an ML-based prognostic variable. It also takes into account the fact that the climate-relevant effects of these feedbacks on the atmosphere typically occur on time scales that are different than the time scale of the changes of the atmosphere on which the AGCM evolves. Method II will be demonstrated by introducing SST as a prognostic variable (Section 3).

In contrast with Method I, the reservoirs for the new prognostic variable are separate from the original reservoirs of the hybrid model. Let $\mathbf{v}_G^{H*}(t)$ be the state vector that represents the global state of the new variable in the hybrid model, and $\breve{\mathbf{v}}_\ell^{H*}(t)$ ($\ell = 1, 2, \ldots, L$) the related local state vectors. The ML-based "prognostic equation" for local vectors ℓ is

$$\breve{\mathbf{v}}_\ell^{H*}(t+\Delta t^*) = \mathbf{W}_\ell^{R*} \tilde{\mathbf{r}}_\ell^{*}(t+\Delta t^*), \tag{10}$$

where

$$\mathbf{r}_\ell^{*}(t+\Delta t^*) = \tanh\left[\mathbf{A}_\ell^{*} \mathbf{r}_\ell^{*}(t) + \mathbf{B}_\ell^{*} \breve{\mathbf{u}}_\ell^{*}(t)\right]. \tag{11}$$

The input vector $\mathbf{u}_\ell^{*}(t)$ includes standardized grid-point values of both the new variable and the original variables, while the "time step" Δt^* is not necessarily equal to Δt (another difference with Method I). For instance, when the newly added prognostic variable evolves on a slower time scale than the atmospheric prognostic variable (e.g., the SST), $\Delta t^* > \Delta t$, and the interactions between the new variable and the atmospheric variables are treated as follows: (1) the time $t + n\Delta t$ ($n = 1, 2, \ldots, \Delta t^*/\Delta t - 1$) input from the new prognostic variable to the AGCM and the atmospheric reservoirs are the values at time t; and (2) the time t input from the atmospheric prognostic variables to

the reservoirs of the new prognostic variable are the average values for the "time steps" $t + n\Delta t$ $(n = 0, 1, \ldots, \Delta t^*/\Delta t)$.

The weight matrix $\mathbf{W}_\ell^{R*}$ is computed separately from $\mathbf{W}_\ell^R$ by

$$\mathbf{W}_\ell^{R*} = \mathbf{V}_\ell^{A*}\tilde{\mathbf{R}}_\ell^{*T}\left(\tilde{\mathbf{R}}_\ell^*\tilde{\mathbf{R}}_\ell^{*T} + \beta^{R*}\mathbf{I}\right)^{-1}, \tag{12}$$

where β^{R*} is a regularization parameter, column k of the matrix $\tilde{\mathbf{R}}_\ell^*$ is $\tilde{\mathbf{r}}_\ell^*(k\Delta t^*)$, and column k of the matrix $\mathbf{V}_\ell^{A*}$ is $\breve{\mathbf{v}}_\ell^{A*}(k\Delta t^*)$ (the local vector of training data for time $k\Delta t$).

3 Climate Simulation Experiment

3.1 Experiment Design

The hybrid model is the same as in AEA22, except that precipitation and SST are added as prognostic variables to the two horizontal coordinates of the wind vector, temperature, specific humidity, and the logarithm of the surface pressure. The precipitation variable is defined by $\ln(P/0.001 + 1)$, where P is the cumulative precipitation for the prior 6 h. The fields of the SST, precipitation, and logarithm of the surface pressure are two-dimensional, while the fields of the other variables are three-dimensional. All fields are represented by a $3.75^\circ \times 3.75^\circ$ horizontal grid, while the three-dimensional fields have eight vertical levels at sigma equals 0.95, 0.835, 0.685, 0.51, 0.34, 0.20, 0.095, and 0.025. The $L = 1,152$ local regions for the atmospheric state variables have a $7.5^\circ \times 7.5^\circ$ horizontal footprint and contain all vertical levels. The extended local regions have a horizontal footprint of $15.0^\circ \times 15.0^\circ$ with an overlap of 3.75° (1 grid point) on each side. The climatological mean and standard deviation for the standardization of the components of the local state vectors and input vectors of the reservoirs are computed for the specific variable at the specific vertical level for the extended local region.

The input vectors of the reservoirs for the atmospheric prognostic variables include the standardized values of the atmospheric prognostic variables from the extended local region, plus the incoming solar radiation at the top of the atmosphere. The "time step" for the atmospheric state variables is $\Delta t = 6$ *h*. The other hyper-parameters of the reservoirs for the atmospheric prognostic variables are $D_r = 6000$, $\alpha = 0.5$, $\beta^R = 10^{-4}$, $\beta^P = 1$, $\kappa = 6$, $\varepsilon = 0.2$, ρ increases from 0.3 at the equator to 0.7 at latitude 45° and beyond. A local state vector and reservoir are created for the SST only if the local region includes at least one oceanic grid point. The coordinates of the local state vectors are the standardized SST values at the oceanic grid points. (A similar approach is employed in the standalone parallel RC-based global SST model of Walleshauser and Bollt (2022)). The "time step" for the SST is $\Delta t^* = 168$ h (7 days), which is 28 times longer than Δt. The elements of the input vectors of the reservoirs are the averages of the atmospheric state variables at the lowest model level for the period $[t, t+\Delta t^*]$ and the SST at time t from the extended local region. At grid points over land, the SST elements of the input vectors are set to a predefined constant (land mask) value. A non-standardized SST value $\leq -1^\circ$C is assumed to indicate ice. In a local region where the ocean is permanently covered by ice in the training data, the ocean is assumed to remain covered by ice. In a local region where both water and ice are present in the training data, the phase of sea water is allowed to change, but non-standardized values of the SST that are $< -1^\circ$C at the end of a time step are reset to -1°C. The other hyperparameters for the SST are $D_r^* = 4000$, $\alpha^* = 0.6$, $\beta^{R*} = 10^{-4}$, $\kappa^* = 6$, $\rho^* = 0.9$, $\varepsilon^* = 0.1$. The feedback from the SST to the atmosphere is introduced by replacing the prescribed SST field of SPEEDY with the last predicted values of the SST, which stays constant for 7 days.

The training and verification data are ERA5 reanalyses (Hersbach et al., 2020). The training period is from 0000UTC 1 January 1981 to 0000UTC 1 December 2006. The ERA5 reanalyses from December 2006 are used to keep the reservoirs synchronized with

the atmosphere, and a 70-year simulation experiment (free run without observational input) is started from the ERA5 reanalysis for 0000 UTC 1 January 2007. The hybrid model remains stable and produces a realistic climate for the entirety of the experiment. The hybrid model climatology for the first 40 years of this experiment is compared to the ERA5 climatology for 1981-2020, and the 40-year climatology for a free run with SPEEDY, which is also started from the ERA5 reanalysis for 000UTC 1 January 2007. The prescribed SST field for SPEEDY is the daily varying 40-year ERA5 SST climatology.

3.2 Sudden Stratospheric Warming

The dominant features of stratospheric variability are wintertime events of sudden stratospheric warming (SSW) in the NH. The term SSW refers to a dynamical process in which the normally strong westerly zonal mean flow at the edge of the NH stratospheric polar vortex suddenly turns easterly, which leads to a sudden rise of the polar stratospheric temperature. This rapid change is caused by an unusually strong coupling between the dynamics of the stratospheric and tropospheric flow (Andrews et al., 1987). While SPEEDY would need additional vertical levels above 25 hPa (its current top level) to produce realistic stratospheric dynamics, the hybrid model can produce realistic SSW events (Figure 1). The blue curves and gray shades show, respectively, the calendar-day mean and year-to-year variability of the strength of the zonal flow at the edge of the stratospheric polar vortex (top three panels) and the polar temperature (bottom three panels). From July to December, the stratospheric flow (left panels) first turns from easterly (negative values) to westerly (positive values), and then it gradually strengthens until midwinter, when it starts to weaken and eventually turns easterly again in April. The mean polar temperature gradually decreases from midsummer to midwinter, when it starts to increase to complete the cycle. The variability of the strength of the zonal flow and the polar temperature is low from May to September and high from October to April, with a maximum in midwinter. While both the hybrid model (middle two panels) and SPEEDY (right two panels) can capture the mean trends, the hybrid model somewhat overestimates, while SPEEDY substantially underestimates the variability of the flow. The relationship between the variability of the flow and SSW can be further investigated by using the criteria of Charlton and Polvani (2007) to detect SSW: an event occurs when the stratospheric zonal mean of the zonal wind at 60°N turns easterly and then it turns back to westerly for at least 10 consecutive days. Here, the criteria is applied to the zonal wind at vertical pressure level 25 hPa. For ERA5, the hybrid model, and SPEEDY, there are 0.6, 0.87, and zero SSW events per year, respectively. The examples for an event shown by the red curves in Fig. 1 illustrate that both the speed of the onset and the duration of the SSW are captured realistically by the hybrid model.

3.3 Precipitation Climatology

The prognostic precipitation variable of the hybrid model provides cumulative precipitation values with 6 hourly resolution, while the diagnostic precipitation variable of SPEEDY provides this variable with a monthly resolution. The precipitation model climatologies of Figure 2 are based on these variables. This figure shows that the hybrid model produces lower magnitude precipitation biases than SPEEDY at most locations (top two rows of panels): the 1.29 mm per day global root-mean-square of the bias for SPEEDY is reduced to 0.63 mm per day for the hybrid model, and the absolute value of the largest-magnitude local bias is reduced from 10.50 mm per day to 5.17 mm per day. SPEEDY has a dry bias in the extension regions of the Kuroshio Current and Gulf Stream (two right panels), which is greatly reduced by the hybrid approach (top two middle panels). The bias is also lower for the hybrid model than SPEEDY in mountainous regions (e.g., Rockies, Himalayas) and equatorial South America and Africa. One region where the hybrid model has a larger bias than SPEEDY is the Tropical Pacific, where

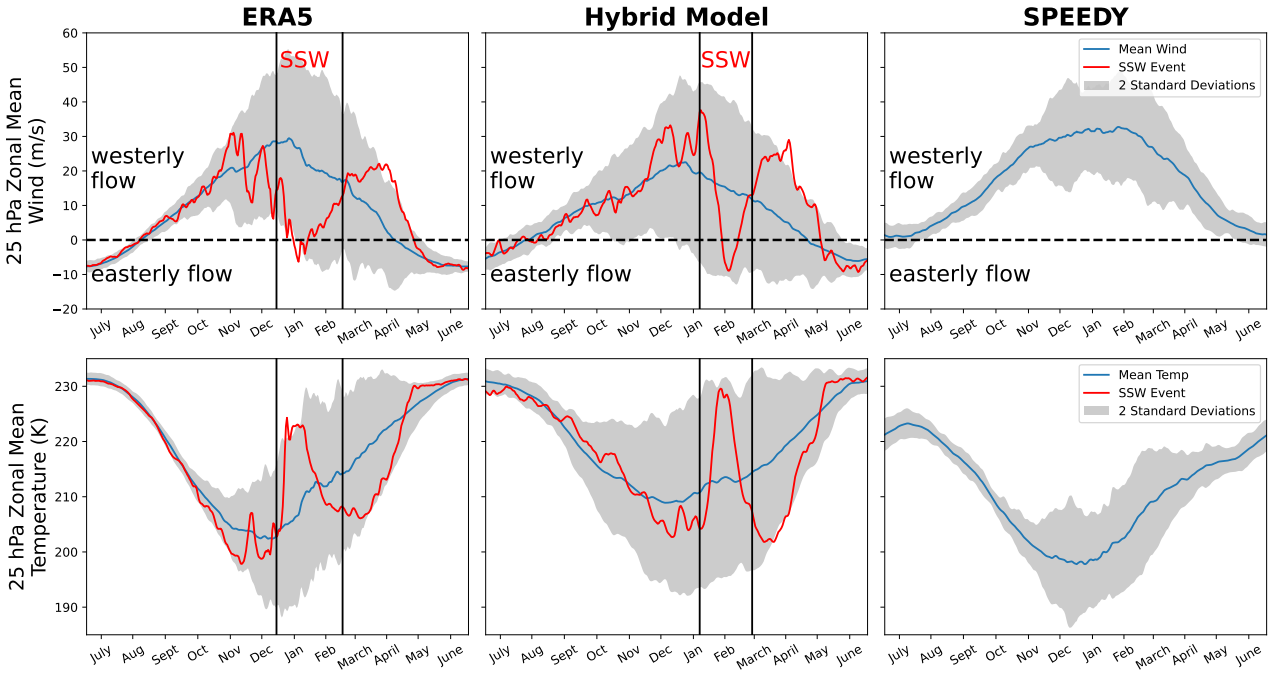

Figure 1. The performance of the hybrid model in capturing SSW. Results are shown for the (left) ERA5 reanalyses, (center) hybrid model, and (right) SPEEDY. Results are shown at the 25 hPa pressure level for (top panels) the mean of the zonal wind component in the 55°N-65°N latitude band, and (bottom panels) the mean temperature north of 60°N. Blue curves show the climatological daily mean, while the gray shading characterizes the annal variability by displaying the range between plus and minus two standard deviations. Positive values of the wind indicate westerly flow, while negative values indicate easterly flow. The red curves show the same diagnostics as the blue curves, except for a particular SSW event rather then the 40-year mean. (No SSW event is detected for SPEEDY.) The event from ERA5 took place in 2013.

it has a wet bias. Interestingly, the hybrid model produces a "double ITCZ", which has also been a persistent problem for physics-based models (Zhang et al., 2019).

In addition to providing improved mean precipitation, the hybrid model produces precipitation events of varying intensity at the correct rates in the range from about 1 mm/6 h to about 7-8 mm/6 h, and it only slightly underestimates the frequency of low and extreme high intensity precipitation (bottom panel).

3.4 SST Climatology and ENSO

The SST prognostic variable (Fig. 3, left panels) has low biases: the global root-mean-square value of the SST bias is 0.43°C, while the largest local values of the bias are in the 1°-2°C range. While the model correctly captures the main regions of largest temporal variability of the SST (Fig. 3, right panels), it tends to somewhat underestimate the variability associated with the western boundary currents and their extension regions, and overestimate the variability associated with ENSO in the Equatorial Pacific near the coast of South America.

The skills and the limitations of the model in capturing climate variability related to ENSO are further illustrated by Fig. 4. Two of the most common metrics used for di-

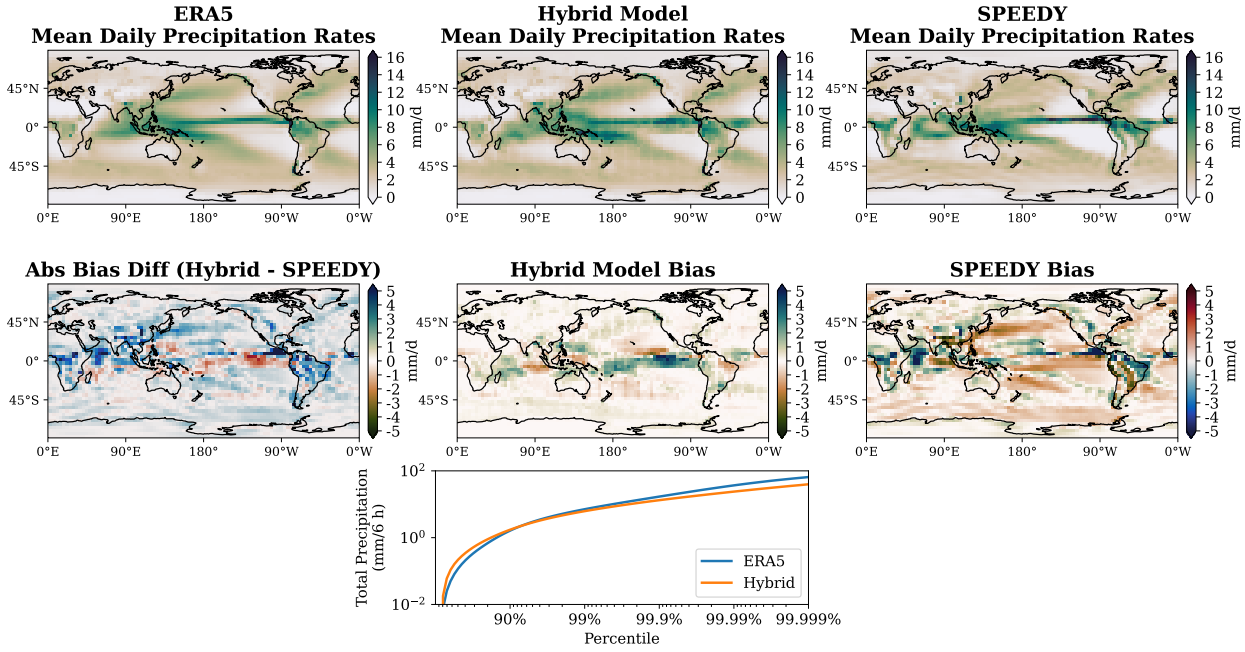

Figure 2. The performance of the hybrid model in capturing the precipitation climatology. Shown is the climatological daily mean precipitation rate for (top left) ERA5, (top center) the hybrid model, and (top right) SPEEDY. Also shown are (middle left) the difference between the biases of the daily precipitation rates for the hybrid model and SPEEDY, and (middle center) the biases of the daily precipitation rates for the hybrid model and (middle right) SPEEDY. Also shown (bottom center) are the rates of occurrence of different precipitation intensities in percentile for (blue) ERA5 and (orange) the hybrid model.

agnosing ENSO phases are the Oceanic Niño Index (ONI) and the Southern Oscillation Index (SOI) for the Niño 3.4 region (5°S-5°N, 120°W-170°W). The model correctly captures the inverse relationship between the smoothed time series of the two indexes (top panel). In addition, the autocorrelation function of the Niño 3.4 SST anomalies for the model is in good agreement with that for the ERA5 reanalyses for the first 6 months of lag (bottom left panel). The model, however, does not capture the timing of the crossover into negative autocorrelation at about 10 months: the model transitions from one phase of ENSO to another with a delay. In addition, the occurrence of ENSO is more regular in the model than in the reanalyses, with too much power at period 5 years, and too little power at period 3, 4, and 7 years (bottom right panel). While some climate models produce too much variability associated with ENSO in the western Tropical Pacific (Menary et al., 2018), the hybrid model does not exhibit such behavior (Fig. 3, bottom right panel).

4 Conclusions

The goal of this paper was to demonstrate that hybridizing an AGCM by incorporating ML can help the model to capture dynamical processes of nature that are missing from climate simulations with the AGCM. For some dynamical processes, this potential can be realized without introducing new prognostic variables in the ML component of the model. This point was illustrated with the process of SSW. Some other processes can be introduced into the model dynamics by adding new ML-based prognostic

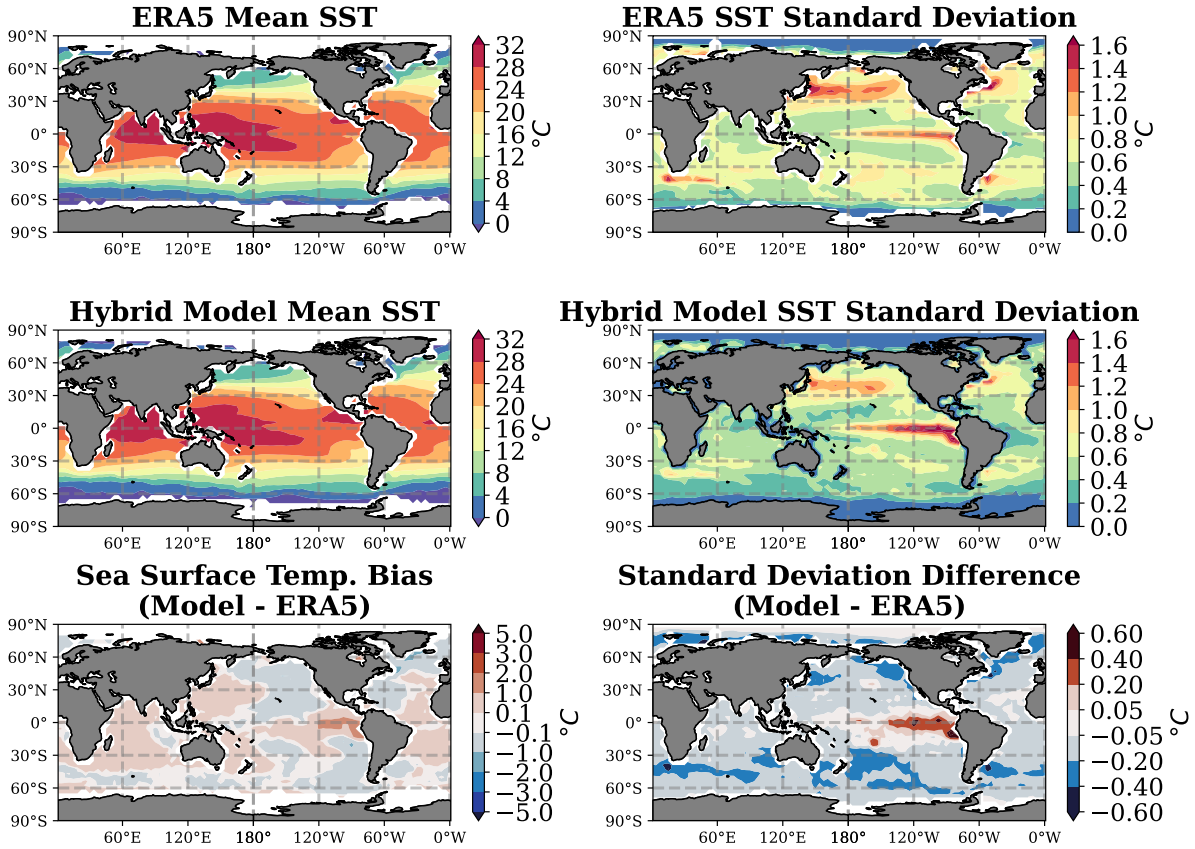

Figure 3. The SST climatology of the hybrid model. Shown are the climatological mean SST for (top left) ERA5, (middle left) the hybrid model, and (bottom left) the difference between the two fields; and the standard deviation of the monthly mean SST for (top right) ERA5 and (middle right) the hybrid model, and (bottom right) the difference between the two fields.

variables. This point was illustrated by two examples. First, the 6-h cumulative precipitation was introduced as a prognostic variable, and it was shown that the model produced a highly realistic climatology for the newly added prognostic variable. Second, SST, which is a prescribed boundary parameter of the AGCM, was turned into a prognostic variable. The SST prognostic variable had highly realistic climatology, and it also had a realistic ENSO signal. Moreover, the hybrid model also correctly captured the related atmospheric surface pressure signal, the indication of a realistic two-way coupling between an oceanic state variable and the model atmosphere. We conjecture that similar two-way coupling could be introduced for other interacting components of the earth system by turning other boundary parameters into prognostic variables.

The one important caveat concerning our conclusions is that they are based on the application of the hybrid approach to an AGCM that has much lower resolution and simpler parameterization schemes than a state-of-the-art AGCM. A state-of-the-art model may leave less room for the improvement of the model representation of some dynamical processes. We still believe that the hybrid approach has a great potential to economically address some of the limitations of even the most sophisticated existing AGCMs.

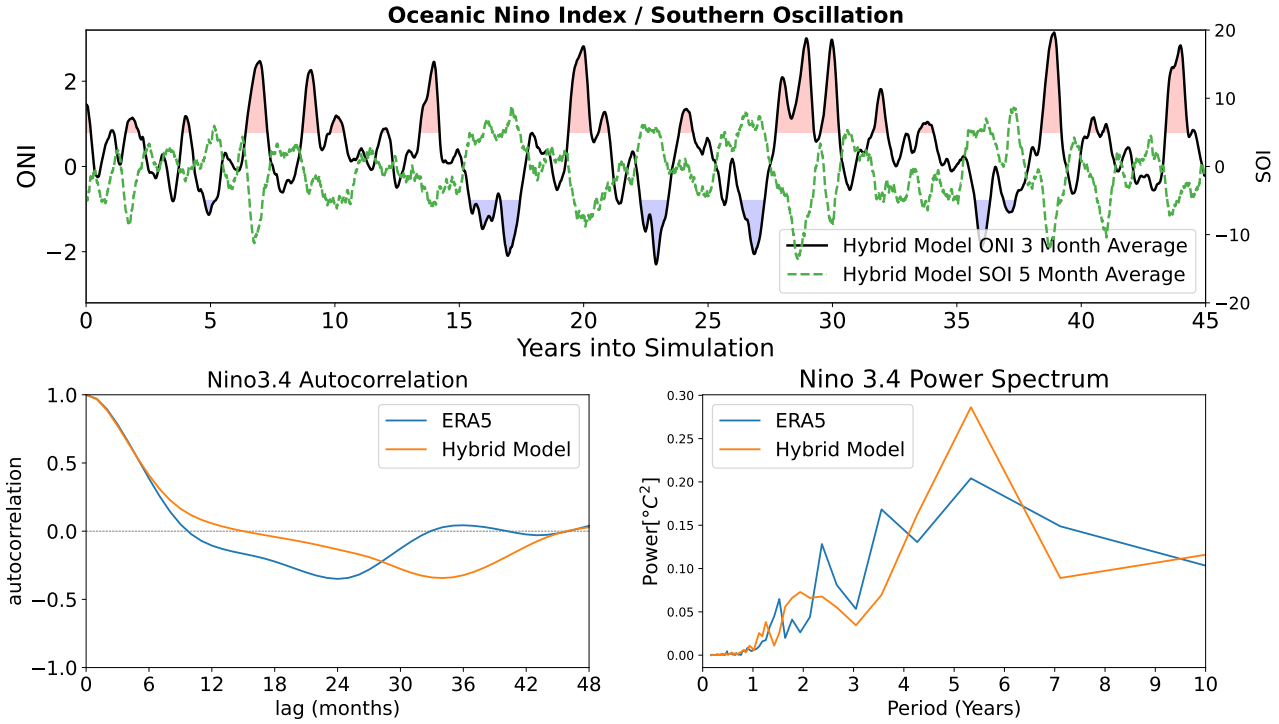

Figure 4. Illustration of the performance of the hybrid model in capturing ENSO. Shown are (top) time series of (solid black) the 3-month running mean of the ONI and (green dashes) the 5-month running mean of the SOI. Red and blue shadings indicate El Niño and La Niña, respectively. Also shown are (bottom left) the autocorrelation functions and (bottom right) power spectra of the Niño 3.4 SST anomalies for (orange) the ERA5 reanalyses and (blue) the coupled model (blue).

Open Research Section

The code to run and analyze the results of the experiments in this study are contained in a GitHub repository https://github.com/Arcomano1234/SPEEDY-ML . The trained weights for the hybrid model used in this study are available online (https://doi.org/10.5281/zenodo.72228).

Acknowledgments

This work was supported by DARPA contract HR00112290035, and it was conducted with the advanced computing resources provided by Texas A&M High Performance Research Computing. Dhruvit Patel provided helpful comments on the manuscript.

References

Andrews, D. G., Holton, J. R., & Leovy, C. B. (1987). Middle atmosphere dynamics. In (Vol. 40). Academic Press.

Arcomano, T., Szunyogh, I., Pathak, J., Wikner, A., Hunt, B. R., & Ott, E. (2020). A machine learning-based global atmospheric forecast model. *Geophysical Research Letters*, *47*, e2020GL087776.

Arcomano, T., Szunyogh, I., Wikner, A., Pathak, J., Hunt, B. R., & Ott, E. (2022). A hybrid approach to atmospheric modeling that combines machine learning

with a physics-based numerical model. *Journal of Advances in Modeling Earth Systems*, *14*(3), e2021MS002712. doi: https://doi.org/10.1029/2021MS002712

Brenowitz, N. D., & Bretherton, C. S. (2018). Prognostic validation of a neural network unified physics parameterization. *Geophysical Research Letters*, *45*, 6289-6298.

Brenowitz, N. D., & Bretherton, C. S. (2019). Spatially extended tests of a neural network parametrization trained by coarse-graining. *Journal of Advances in Modeling Earth Systems*, *11*, 2728-2744.

Charlton, A. J., & Polvani, L. M. (2007). A new look at stratospheric sudden warmings. part i: Climatology and modeling benchmarks. *Journal of Climate*, *20*(3), 449-469. doi: 10.1175/jcli3996.1

Chattopadhyay, A., Subel, A., & Hassanzadeh, P. (2020). Data-driven super-parameterization using deep learning: Experimentation with multiscale lorenz 96 systems and transfer learning. *Journal of Advances in Modeling Earth Systems*, *12*(11), e2020MS002084. doi: https://doi.org/10.1029/2020MS002084

Clark, S. K., Brenowitz, N. D., Henn, B., Kwa, A., McGibbon, J., Perkins, W. A., ... Harris, L. M. (2022). Correcting a 200 km resolution climate model in multiple climates by machine learning from 25 km resolution simulations. *Journal of Advances in Modeling Earth Systems*, *14*(9), e2022MS003219. doi: https://doi.org/10.1029/2022MS003219

Farchi, A., Laloyaux, P., Bonavita, M., & Bocquet, M. (2021). Using machine learning to correct model error in data assimilation and forecast applications. *Quarterly Journal of the Royal Meteorological Society*, *147*(739), 3067-3084. doi: https://doi.org/10.1002/qj.4116

Gentine, P., Pritchard, M., Rasp, S., Reinaudi, G., & Yacalis, G. (2018). Could machine learning break the convection parameterization deadlock? *Geophysical Research Letters*, *45*, 5742-5751.

Hersbach, H., Bell, B., Berrisford, P., Hirahara, S., Horányi, A., Muñoz-Sabater, J., ... Thépaut, J.-N. (2020). The ERA5 global reanalysis. *Quarterly Journal of the Royal Meteorological Society*, *146*(730), 1999-2049. doi: https://doi.org/10.1002/qj.3803

Jaeger, H. (2001). The "echo state" approach to analysing and training recurrent neural networks-with an erratum note. *Bonn, Germany: German National Research Center for Information Technology GMD Technical Report*, *148*.

Kucharski, F., Molteni, F., & Bracco, A. (2006). Decadal interactions between the western tropical pacific and the north atlantic oscillation. *Climate Dynamics*, *26*(1), 79-91.

Lukoševičius, M. (2012). A practical guide to applying echo state networks. In G. Montavon, G. B. Orr, & K.-R. Müller (Eds.), *Neural networks: Tricks of the trade: Second edition* (p. 659-686). Berlin, Heidelberg: Springer Berlin Heidelberg.

Lukoševičius, M., & Jaeger, H. (2009). Reservoir computing approaches to recurrent neural network training. *Computer Science Review*, *3*(3), 127-149.

Menary, M. B., Kuhlbrodt, T., Ridley, J., Andrews, M. B., Dimdore-Miles, O. B., Deshayes, J., ... Xavier, P. (2018). Preindustrial control simulations with hadgem3-gc3.1 for cmip6. *Journal of Advances in Modeling Earth Systems*, *10*(12), 3049-3075. doi: https://doi.org/10.1029/2018MS001495

Molteni, F. (2003). Atmospheric simulations using a GCM with simplified physical parametrizations. I: model climatology and variability in multi-decadal experiments. *Climate Dynamics*, *20*(2), 175-191.

Pathak, J., Hunt, B., Girvan, M., Lu, Z., & Ott, E. (2018). Model-free prediction of large spatiotemporally chaotic systems from data: A reservoir computing approach. *Physical Review Letters*, *120*(2), 024102.

Pathak, J., Wikner, A., Fussell, R., Chandra, S., Hunt, B. R., Girvan, M., & Ott, E. (2018). Hybrid forecasting of chaotic processes: Using machine learning in

conjunction with a knowledge-based model. *Chaos*, *28*(4), 041101.

Rasp, S., Pritchard, M. S., & Gentine, P. (2018). Deep learning to represent subgrid processes in climate models. *Proceedings of the National Academy of Sciences*, *115*, 9684-9689.

Walleshauser, B., & Bollt, E. (2022). Predicting sea surface temperatures with coupled reservoir computers. *Nonlin. Processes Geophys.*, *29*(3), 255-264. doi: 10.5194/npg-29-255-2022

Watt-Meyer, O., Brenowitz, N. D., Clark, S. K., Henn, B., Kwa, A., McGibbon, J., ... Bretherton, C. S. (2021). Correcting weather and climate models by machine learning nudged historical simulations. *Geophysical Research Letters*, *48*(15), e2021GL092555. doi: https://doi.org/10.1029/2021GL092555

Wikner, A., Pathak, J., Hunt, B., Girvan, M., Arcomano, T., Szunyogh, I., ... Ott, E. (2020). Combining machine learning with knowledge-based modeling for scalable forecasting and subgrid-scale closure of large, complex, spatiotemporal systems. *Chaos*, *30*(5), 053111.

Zhang, G. J., Song, X., & Wang, Y. (2019). The double ITCZ syndrome in GCMs: A coupled feedback problem among convection, clouds, atmospheric and ocean circulations. *Atmospheric Research*, *229*, 255-268. doi: https://doi.org/10.1016/j.atmosres.2019.06.023